Experiments on vortex dynamics in pure electron plasmas*

C. F. Driscoll† and K. S. Fine
University of California at San Diego, La Jolla, California 92093

(Received 6 December 1989; accepted 21 February 1990)

Magnetically confined columns of electrons are excellent experimental manifestations of two-dimensional (2-D) vortices in an inviscid fluid. Surface charge perturbations on the electron column (diocotron modes) are equivalent to surface ripples on extended vortices; and unstable diocotron modes on hollow electron columns are examples of the Kelvin–Helmholtz instability. Experiments demonstrate that the stable and unstable modes are distinct and may coexist, having different frequencies and radial eigenfunctions. For azimuthal mode number $l = 1$, an exponentially unstable mode is observed on hollow columns, in apparent contradiction to 2-D fluid theory. For $l = 2$, a similar unstable mode is observed, consistent with fluid theory. These diocotron instabilities on hollow columns saturate with the formation of smaller vortex structures, and radial transport is determined by the nonlinear interaction of these secondary vortices. The vortex pairing instability has been observed for isolated, well-controlled vortices, and the instability is found to depend critically on the vortex separation distance.

I. INTRODUCTION

It has been known for 25 years that the two-dimensional (2-D) drift-Poisson equations governing a magnetized electron column are isomorphic to the Euler equations governing a constant density inviscid fluid.[1,2] However, this has been treated as little more than a curiosity, and is not mentioned in standard texts on non-neutral plasmas.[3,4] Here, we shall try to demonstrate that electron columns are excellent experimental manifestations of 2-D vortices, with interesting consequences for both fluid theory and plasma experiments.

This isomorphism implies that surface charge perturbations on electron columns, called diocotron modes,[1-11] are equivalent to the surface ripples on extended vortices first studied by Kelvin.[12,13] The electron system has a large experimental advantage in that we can directly measure the charge density $n(r,\theta,t)$, which is proportional to the vorticity of the flow. When the radial density profile is monotonically decreasing, the Rayleigh stability criterion[3,14] demonstrates that all modes are stable. When the density profile is nonmonotonic (i.e., "hollow"), the unfavorable shear in the rotation velocity gives rise to unstable diocotron modes, which are examples of the Kelvin–Helmholtz instability.[15]

Theory approximations based on "step profiles" are useful for obtaining simple answers, but lead to the misconception that the stable mode becomes unstable as the profile becomes hollow. Experimentally, we observe that the stable and unstable modes are distinct and may propagate simultaneously.[9,11] The measurements completely characterize the modes, showing they have different radial eigenfunctions as well as different frequencies.

Unstable diocotron modes were perhaps the first striking manifestation of collective instabilities on non-neutral systems, being readily observable as the filamentation of hollow beams.[16] Similarly, the Kelvin–Helmholtz instability is readily observed in a variety of sheared fluid flows.[15] Nevertheless, there has been surprisingly little experimental analysis of growth rates and eigenfunctions for detailed comparison to theory. Our preliminary measurements of the unstable diocotron mode with azimuthal mode number $l = 2$ show agreement with 2-D fluid theory.[9] However, these experiments have deferred to investigation of a surprising contradiction observed for $l = 1$ perturbations.

For $l = 1$, linear mode theory predicts that there are no exponentially unstable diocotron modes in our geometry (which has no conductor at $r = 0$).[1,3] However, a recent linear initial value analysis based on the Laplace transform predicts that there is a subtle instability that grows asymptotically as $\sqrt{t}$.[17] Experimentally, we observe a robust exponential instability that is basically similar to the unstable $l = 2$ mode.[11] This discrepancy may indicate that the theory is inadequate, or that experimental subtleties such as finite length must be considered. In either case, this new instability has an important effect on a realistic 2-D vortex system.

The diocotron instabilities on hollow columns saturate with the formation of smaller vortices and filamentary structures. Radial transport to a stable, monotonically decreasing density profile is then the result of nonlinear interactions among these smaller vortices, with a prominent interaction being the vortex pairing instability.[18-20] There are also interesting turbulence and noise questions associated with this process.[9]

We are able to study the vortex pairing instability in detail by starting with two well-formed, isolated vortices. We find that the time required to merge varies dramatically from less than one orbit period to over 10^4 orbit periods as the separation between the vortices varies from 1.8 to 2.0 vortex diameters. Here, an advantage of the electron system becomes apparent: the internal electron viscosity is very low and there are no radial or axial boundary layers to dissipate the vortices. Unlike conventional fluids that "spin down" in 10 to 30 orbit periods,[19] the electron system shows little dissipation even on time scales of 10^4 orbits. The electron sys-

*Paper 4I5, Bull. Am. Phys. Soc. **34**, 2001 (1989).
†Invited speaker.

 0899-8221/90/061359-08$02.00

tem may thus offer the best experimental data on this fundamental vortex interaction process.

II. ELECTRON CONTAINMENT

The pure electron plasmas are contained in a grounded conducting cylinder, as shown in Fig. 1. A uniform axial magnetic field ($B_z = 375$ G) provides radial confinement and negative voltages applied to end cylinders provide axial confinement. The apparatus is operated in an inject/manipulate/dump cycle. For injection, the leftmost cylinder is briefly grounded, allowing electrons to enter from the negatively biased tungsten filament source. The trapped electrons can be contained for hundreds of seconds,[4,21] and can be manipulated in a variety of ways. Typically, we manipulate the plasma to create the desired "initial condition" then study the resulting evolution.

At any time t during this evolution, we can obtain the plasma density by grounding the rightmost cylinder, thereby dumping the plasma. We measure the charge $Q(r,\theta,t)$ that flows along B_z through a collimator hole of area $A_h = \pi\,(1.6\ \text{mm})^2$, giving the z-averaged density[10]

$$n(r,\theta,t) \equiv \int dz\, \frac{\tilde{n}(r,\theta,z,t)}{L_p} = \frac{Q(r,\theta,t)}{(-eA_h L_p)}. \tag{1}$$

Only one density measurement is obtained on each machine cycle. We obtain the temporal dependence by varying the evolution time t and the spatial dependence by varying the position r of the radially scanning collimator hole, and the phase θ of the initial condition. Of course, this imaging process relies on a high cycle-to-cycle reproducibility in the plasma initial conditions; typically we have less than 0.1% variations in the measured Q at a given point and time.

The plasmas considered here have local densities $\tilde{n} \approx 5\times 10^6\ \text{cm}^{-3}$ out to a (half-density) radius $R_p \approx 1$–2 cm over an axial length $L_p \approx 30$ cm, and are contained in a cylinder of radius $R_w = 3.81$ cm. The unneutralized space charge gives a radial electric field $E_r \lesssim -7$ V/cm, resulting in an $E\times B$ rotation frequency of $f_E \lesssim 140$ kHz. The electrons have a characteristic thermal energy $kT \lesssim 1$ eV, giving a cyclotron radius $r_c \lesssim 60\ \mu$m, and an axial "bounce" rate $f_b \equiv v_\parallel / 2L_p \gg f_E$.

The plasma column can also be diagnosed and manipulated using isolated 60° sectors of the wall as antennas. Any azimuthal or axial variations in the electron density induce variations in the image charges on the wall sectors and these waves can be detected with high sensitivity. Conversely, voltages applied to the wall sectors induce drifts in the electrons, thereby launching waves. Applied voltages of $\geqslant 1$ V can induce significant (i.e., readily detected) density waves in about 1 μsec. Alternately, smaller voltages may be applied phase coherent with an internal wave using standard positive or negative feedback techniques over larger times.

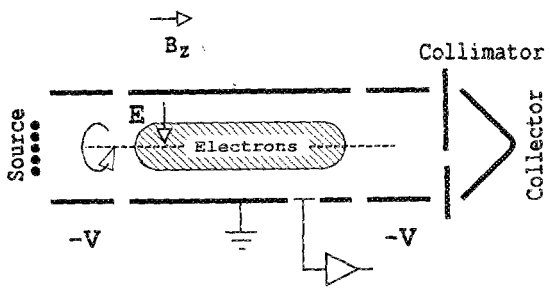

FIG. 1. The cylindrical containment apparatus.

The electron column is easily manipulated in the axial direction by varying the containment voltages on various cylindrical electrodes. There are actually seven containment cylinders, as opposed to the three shown schematically in Fig. 1. If a substantial negative voltage is applied to the central ring, the electron column can be "cut in half," giving two independent columns separated axially. This technique is used to create the two vortices discussed later. Alternately, if the containment voltage on an end cylinder is made less negative, some electrons will escape axially in a time $\leqslant 1\ \mu$sec. The electrons escape preferentially from near $r = 0$, where the space-charge potential is most negative and the containment voltage is least negative. This technique is used to create the "hollow" plasma initial conditions discussed later.

III. DRIFT DYNAMICS

The electron dynamics can be approximated by the two-dimensional guiding center theory. Here, the axial bouncing of the individual electrons averages over any z variations at a rate fast compared to r-θ motions. The r-θ motions of interest arise as a result of particle drifts, which can be treated by the guiding center equations, since the cyclotron orbit size is small.

The 2-D drift-Poisson equations for the evolution of the electron column are isomorphic to the 2-D Euler equations for an inviscid fluid of uniform density ρ.[1,2] This isomorphism is displayed in Fig. 2. The electrostatic potential ϕ arises from the charge density n through Poisson's equation, and the resulting $E\times B$ drift velocities give incompressible flow. (The drift velocity is well defined even where there are

2D Drift-Poisson	2D Euler, ρ = constant
Poisson: $\nabla^2\phi = 4\pi e n$	
E×B Drifts: $\mathbf{v} = -\frac{c}{B}\nabla\phi\times\hat{z}$	Stream Function: $\mathbf{v} \equiv -\nabla\psi\times\hat{z}$
Vorticity: $\Omega \equiv \nabla\times\mathbf{v} = \nabla^2\phi\,\frac{c}{B}\hat{z} = n\,\frac{4\pi e c}{B}\hat{z}$	Vorticity: $\Omega \equiv \nabla\times\mathbf{v} = \nabla^2\psi\,\hat{z}$
Continuity: $\frac{\partial n}{\partial t} + \mathbf{v}\cdot\nabla n = 0$; $\frac{\partial\Omega}{\partial t} + \mathbf{v}\cdot\nabla\Omega = 0$	Momentum: $\frac{\partial\mathbf{v}}{\partial t} + \mathbf{v}\cdot\nabla\mathbf{v} = -\frac{1}{\rho}\nabla p$; $\frac{\partial\Omega}{\partial t} + \mathbf{v}\cdot\nabla\Omega = 0$

$$\phi \leftrightarrow \psi$$
$$\mathbf{v} \leftrightarrow \mathbf{v}$$
$$n, \Omega \leftrightarrow \Omega$$

FIG. 2. The 2-D drift-Poisson equations are isomorphic to the 2-D Euler equations for a constant density fluid.

no electrons.) This is equivalent to incompressible fluid flow characterized by a streamfunction ψ. The vorticity Ω of the flow is then proportional to $\nabla^2\phi$ (or $\nabla^2\psi$). In the electron system only, this vorticity is proportional to the density n, which we measure directly. The continuity equation for electrons and the momentum equation for the fluid then both give the same evolution equation, i.e., that the convective derivative of the vorticity is zero. The boundary conditions are also equivalent, namely, $\phi = \text{const}$ and $\psi = \text{const}$ on the cylindrical walls.

Thus, an initial distribution of electrons $n(r,\theta,t=0)$ in a cylinder with vorticity $\Omega \propto n$ will evolve exactly the same as an initial distribution of vorticity Ω in a uniform fluid such as water. For example, a single column of electrons in our apparatus is equivalent to an extended vortex in a tube of water. If the vortex is centered and azimuthally symmetric, it will have a stationary flow field $v_\theta(r)$. Outside the region of vorticity, the flow falls off as $v_\theta \propto 1/r$. This arises naturally from Poisson's equation in the electron system, since $E_r \propto 1/r$ outside the charge column.

One advantage of the electron experiments for testing 2-D fluid theory is that the electron system tends to remain two dimensional because of the magnetic field. Another advantage is that the electron column has low internal viscosity and has no boundary layers at the cylindrical walls or ends. The time for internal viscosity to act is typically 10 sec,[21] compared to the 10 μsec time scale for the drift motions of interest here. Further, the $E \times B$ drift velocity v_θ may be large at the wall, but since there are typically no electrons near the walls, one has a free-slip boundary condition. Of course, small effects on the electron dynamics (such as finite cyclotron radius and finite z-length effects) have been ignored here.

The evolution of the 2-D drift system is constrained by three conserved quantities.[3,4] These are the total number of particles,

$$N_L \equiv \int\int d\theta r\, dr\, n(r,\theta,t); \tag{2}$$

the angular momentum,

$$P_\theta \equiv \int\int d\theta r\, dr\left(\frac{-eB}{2c} r^2\right) n(r,\theta,t); \tag{3}$$

and the electrostatic energy,

$$E \equiv \int\int d\theta\, r\, dr\left(-\frac{1}{2} e\phi(r,\theta,t)\right) n(r,\theta,t). \tag{4}$$

Of course, these quantities are all per unit axial length in a 3-D system. In fluid dynamics the corresponding quantities would be called the total circulation, the total angular impulse, and the excess kinetic energy.[20]

IV. LINEAR WAVE THEORY

Linear wave theory treats $k_z = 0$ modes as surface charges (or vorticity) rotating on the surface of a centered, symmetric charge (or vorticity) column. That is,

$$n(r,\theta,t) \equiv n_0(r) + \sum_l \delta n_l(r,t) e^{il\theta}, \tag{5}$$

$$\delta n_l(r,t) \equiv \sum_q \delta n_{lq}(r) A_{lq}(t), \tag{6}$$

with

$$A_{lq}(t) = e^{-i2\pi f_{lq} t} e^{\gamma_{lq} t} \tag{7}$$

for an eigenmode.

Linearizing the evolution equations of Fig. 2 gives the eigenvalue equation,[2,3] which is most conveniently written in terms of the perturbed potential $\delta\phi_{lq}(r)$ corresponding to $\delta n_{lq}(r)$:

$$\left(\frac{1}{r}\frac{\partial}{\partial r} r \frac{\partial}{\partial r} - \frac{l^2}{r^2}\right)\delta\phi_{lq} = \frac{-2ecl\, \partial n_0/\partial r}{rB\,[f_{lq} + i\gamma_{lq}/2\pi - l f_E(r)]}\,\delta\phi_{lq}, \tag{8}$$

where

$$f_E(r) \equiv \frac{cE_0(r)}{2\pi rB} = \frac{ec}{\pi r^2 B}\int_0^r 2\pi r'\, dr'\, n_0(r') \tag{9}$$

is the $E \times B$ rotation frequency of the unperturbed equilibrium.

As early as 1880, Kelvin noted "A Disturbing Infinity in Lord Rayleigh's Solution..."[22] when the denominator becomes zero at r_s, where $f_{lq} = l f_E(r_s)$. This difficulty can be delayed by considering only "step" profiles, with $\partial n_0/\partial r = 0$ except at discrete steps. One then obtains as many modes as there are steps, and the mode frequencies are either real or occur in complex conjugate pairs.[2,3] However, this result seems to have little utility in predicting the number and types of modes in experiments.

If a continuous profile is approximated by a single step profile (a vortex "patch"), as shown in Fig. 3(a), a single stable mode is predicted, with frequency[3,7]

$$f_{ls} = f_E(0)\left[l + (R_p/R_w)^{2l} - 1\right].$$

These modes were first studied by Kelvin[12] as ripples on the surface of a vortex in the absence of a bounding wall, i.e., with $R_w = \infty$. For the case where there is a boundary wall, the $l = 1$ mode is particularly simple,[1] with frequency

$$f_{1s} = f_E(R_w) = ceN_L/\pi R_w^2 B, \quad \gamma_{1s} = 0, \tag{10}$$

and eigenfunction

$$\delta n_{1s}(r) = D\frac{\partial n_0}{\partial r}. \tag{11}$$

Note that the frequency depends only on the total number of particles (per unit length) N_L rather than on the profile $n_0(r)$; and there are no resonant particles, since $r_s = R_w$.

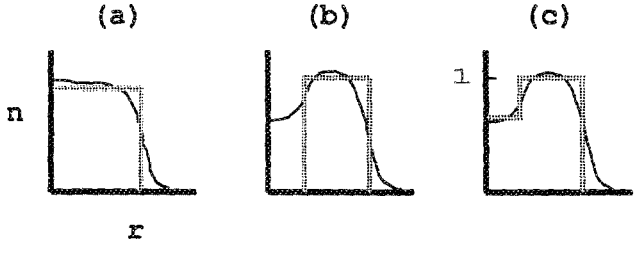

FIG. 3. "Step profile" approximations to continuous density profiles.

For $l > 1$, Eq. (8) must be integrated numerically, and there may be resonant particles.

V. STABLE DIOCOTRON MODES

The simplest dynamical motion of the electron column is the stable $l = 1$ diocotron mode.[1,5,6,10] This mode is merely the entire plasma column displaced a distance D off the cylindrical axis. In this case, the column orbits around the cylindrical axis as well as rotating about its own center. Experimentally, this mode is observed at the predicted frequency, and persists undamped for more than 10^5 orbits.[10] The 2-D linear theory predicts no damping of this mode, whereas some finite-length theories[7] predict weak damping (which is not observed). Previous observations of damping of this mode[5] were apparently caused by loss of plasma containment.

When the electron column is pushed a long distance off center, linear theory is inapplicable, and the motion is more properly referred to as a nonlinear dynamical state of the system. Figure 4 shows an example of the z-integrated electron density measured at a particular phase of a large amplitude $l = 1$ diocotron mode.[10] Note that the electron column is oval rather than circular, equivalent to the distortion of a fluid vortex interacting with a wall.[23] Even at these large amplitudes, no damping of this mode is observed. Thus, the vortex would be stationary in a frame rotating at the wave frequency f_{1s}. This implies that the density contours coincide with the potential contours, since in $E \times B$ flow the density is convected along potential contours. The nonlinear dynamical state is therefore determined by

$$\nabla^2 \phi_f(r,\theta) = 4\pi e n(r,\theta) = F(\phi_f), \tag{12}$$

where ϕ_f is the potential in the rotating frame and F is an unknown function.

We find that the oval distortion of the column is proportional to the mode amplitude squared, as is the shift in frequency of the mode.[10] Figure 5 shows the relative quadrupole moment q_2 and the frequency shift $(f - f_0)/f_0$. Here, f_0 is the small amplitude mode frequency. The frequency shift arises because (1) the column is closer to its image than a linear model assumes, and (2) the shape distortion modifies the image charge distribution. The experimental results corroborate theory and computational models.

The stable $l = 2$ diocotron mode is the next simplest conceptually. This mode is an elliptically distorted column rotating about the cylindrical axis. Kirchhoff generalized the $l = 2$ linear mode to large amplitude by demonstrating analytically that an elliptical vortex patch is an unchanging rotating solution for arbitrarily large ellipticity.[24] Historically, this mode has been observed to be damped, because the profile $n_0(r)$ was nonzero at the resonant radius r_s.[5] This damping is the spatial analog of Landau damping, here depending on $\partial n_0/\partial r$ rather than on $\partial f_0/\partial v$.[2] With profiles that fall to zero sufficiently rapidly, the mode is observed to be essentially undamped.

Figure 6 shows the electron density in the presence of an $l = 2$ diocotron mode of two different amplitudes. The smaller amplitude mode of Fig. 6(a) is experimentally undamped, since the electron density falls to zero inside r_s. Of course, for large amplitude modes, r_s varies with θ. When the mode is driven to larger amplitude, the column becomes more eccentric, and some electrons become resonant with the wave. The resonant electrons are transported in r and θ, forming the low-density filamentary arms and resulting in

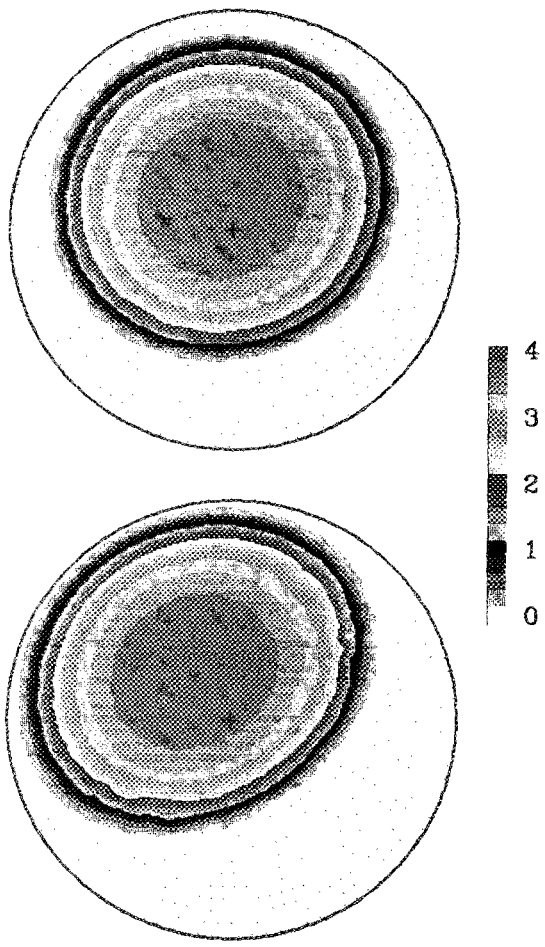

FIG. 4. Measured density $n(r,\theta)$ phase coherent with a stable $l = 1$ diocotron mode of two different amplitudes. Colors represent density on a linear scale of 10^6 cm^{-3}.

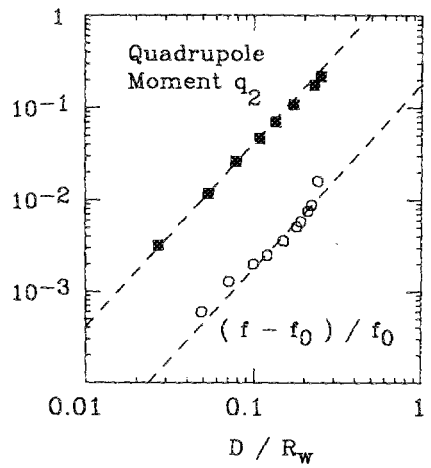

FIG. 5. Quadrupole moment q_2 (measuring ellipticity) and frequency shift versus displacement D for the $l = 1$ mode of Fig. 4.

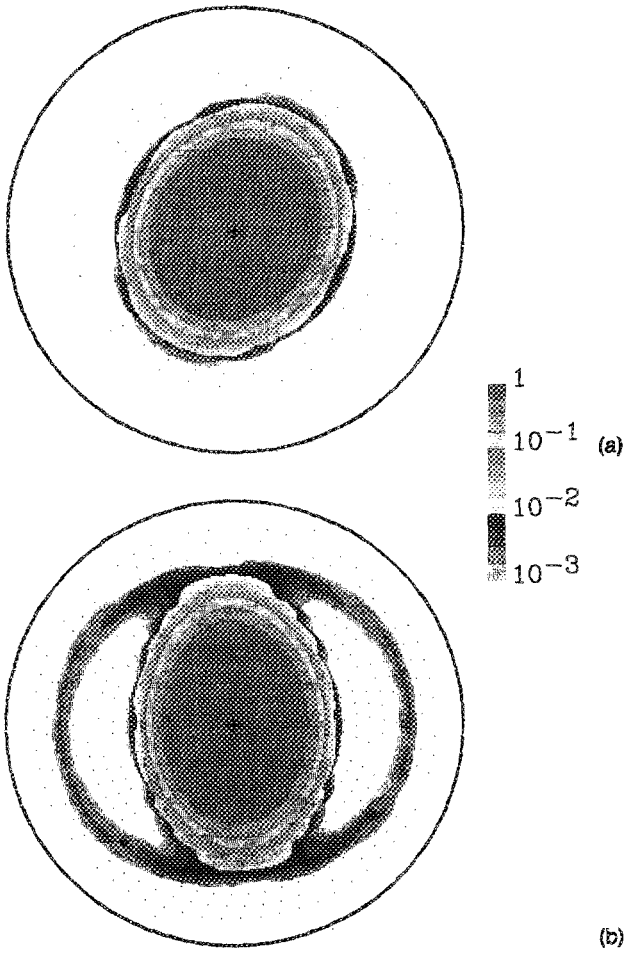

FIG. 6. Measured density $n(r,\theta)$ phase coherent with a stable $l = 2$ diocotron mode of two different amplitudes. Colors represent density on a logarithmic scale.

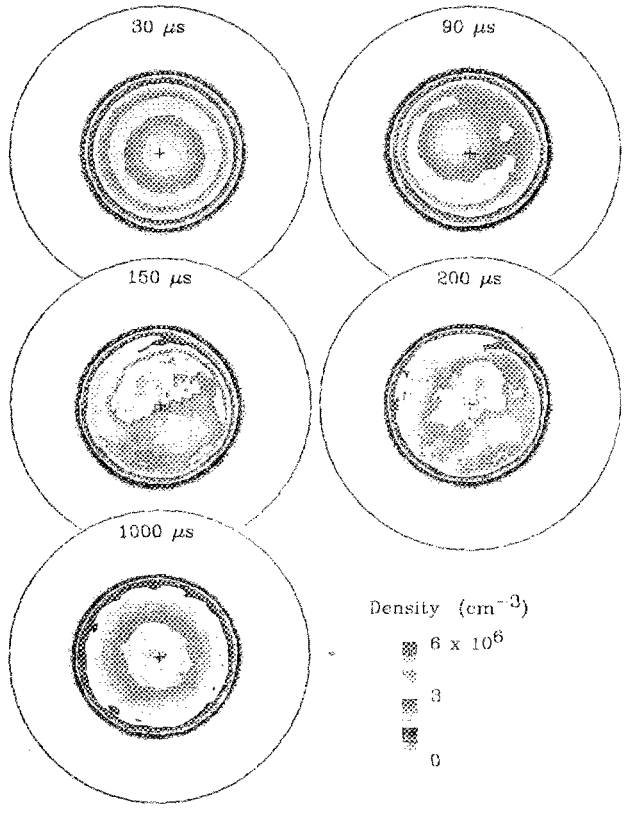

FIG. 7. Measured density $n(r,\theta)$ at five times in the evolution of a hollow column that had a small $l = 1$ perturbation at $t = 0$.

some wave damping. However, there are a finite number of electrons that can participate in the damping, and the process soon saturates. The density configuration of Fig. 6(b) rotates unchanged for hundreds of wave periods, being the saturated state of nonlinear wave damping.

VI. UNSTABLE DIOCOTRON MODES

When the charge density profile $n_0(r)$ is nonmonotonic (i.e., at least partially "hollow"), unstable diocotron modes may appear. Experimentally, these unstable modes are found to be distinct from the stable modes. That is, for any given l, the stable and unstable modes coexist, with distinct frequencies and radial eigenfunctions. This distinction has been missed historically due to reliance on step profile approximations. Furthermore, we observe a robust exponential instability for $l = 1$ where none is predicted.

Figure 7 shows the evolution of a partially hollow electron column when a small $l = 1$ seed exists at $t = 0$.[11] The initial seed asymmetry has two components: the center of mass (c.m.) of the plasma column is displaced off the cylindrical axis, and the central density minimum is not centered in the plasma. We observe that the c.m. orbits about the axis with constant orbit size (this is the stable mode). Similarly, the low-density region orbits about the c.m. but it is spiraling outward with time (this is the unstable mode). The unstable mode also causes the high-density ring to collapse in θ into a high-density region, as shown at $t = 150$ μsec. Eventually, the high-density region moves to the center and the low-density region spreads out in θ at an appropriate radius, as shown at $t = 200$ μsec. Most θ variations (with respect to the c.m.) have been eliminated by $t = 1000$ μsec.

The initial stages of this evolution can be analyzed from the perspective of linear modes, and our data for $n(r,\theta,t)$ characterizes the $k_z = 0$ modes rather completely. The Fourier transform of Eq. (5) gives $\delta n_l(r,t)$ directly from the density measurements. We observe that two frequency components are present in $\delta n_1(r,t)$, and that these frequencies do not vary with radius, consistent with Eqs. (6) and (7). Thus, the $l = 1$ data component can be computationally fit to a sum of two modes, and this least-squares fit determines the mode frequencies f_{1q}, growth rates γ_{1q}, and radial eigenfunctions $\delta n_{1q}(r)$.

Figure 8 shows the amplitudes and phases of the radial eigenfunctions of the stable and unstable modes, δn_{1s} and δn_{1u} (normalized to unity), obtained from an evolution similar to that of Fig. 7. The eigenfunction δn_{1s} represents the stable orbit of the entire hollow plasma column about the cylindrical axis: the amplitude and phase are well approximated by $\delta n_{1s}(r) = \partial n_0/\partial r$, as predicted by linear theory.[1] This mode appears to have the same general characteristics for either monotonic or hollow density profiles, with a frequency $f_E(R_w)$.

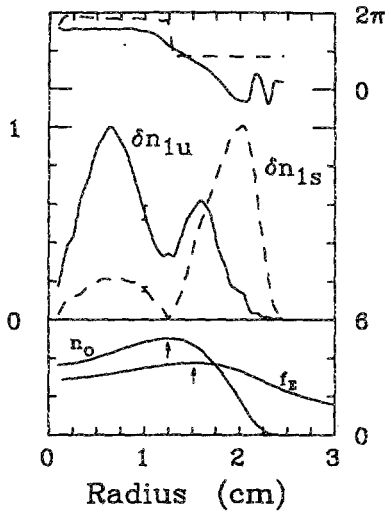

FIG. 8. Stable and unstable $l = 1$ eigenfunctions $\delta n_{1s}(r)$ and $\delta n_{1u}(r)$ displayed as complex amplitudes and phases. Also shown are the equilibrium profile $n_0(r)$ (units 10^6 cm^{-3}) and the $E \times B$ rotation frequency $f_E(r)$ (units 40 kHz).

The unstable mode arises only for density profiles that are at least partially hollow. The unstable mode frequency f_{1u} equals the maximum of $f_E(r)$, to within the experimental accuracy of $\pm 3\%$ in determining $f_E(r)$. Interestingly, this mode is largely self-shielding: the electric field arising from the mode is essentially zero outside the plasma. That is, no wall-sector signal is received from the growing mode, and the electric field eigenfunction $\delta\phi_{1u}(r)$ calculated from the measured $\delta n_{1u}(r)$ is essentially zero outside the plasma.

Figure 9 shows the magnitude of the unstable mode amplitude A_{1u} versus time for two initial seed perturbations differing by 30 dB, i.e., $D = 850\ \mu$m and $D = 27\ \mu$m. (The upper curve is the evolution of Fig. 7.) In both cases, the perturbation initially exhibits what appears to be exponential growth. For the smallest initial perturbation, this exponential growth covers more than two decades. The instability e-folds in about six wave periods, and appears to be a linear process, as evidenced by the parallel growth curves in Fig. 9. Further, the mode saturates at the expected level, representing θ variations from the minimum to the maximum density. After this time, nonlinear vortex dynamics and the effects of rotational shear eventually eliminate the θ variations.

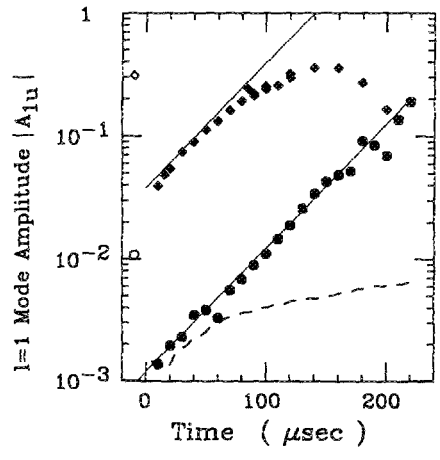

FIG. 9. Amplitude of the unstable $l = 1$ mode versus time for two different amplitudes of initial $l = 1$ perturbation. The upper curve corresponds to Fig. 7. For comparison, an initial value theory integration is shown as the dashed line. Hollow symbols are the initial amplitudes $|A_{1s}|$ of the stable mode, which remains essentially constant with time.

Also shown for reference in Fig. 9 is the theoretically predicted $l = 1$ growth.[17] This curve was obtained by numerically integrating a linear Laplace transform solution that started from initial conditions similar to the experimental initial conditions. Asymptotically, the initial value integration gives a perturbation proportional to $t^{1/2}$, i.e., algebraic growth.

Although the differences between experiment and theory here are large, there are intriguing similarities. The early time instability growth is seen to be similar. Further, the time-asymptotic theory perturbation is self-shielding,[17] as is observed experimentally at all times.[11] However, the relation between the experimental and theoretical instabilities is not presently understood.

For $l = 2$, an exponentially unstable mode is observed for a wide range of hollow profiles,[9] and these results are basically consistent with 2-D theory predictions. Figure 10 displays $n(r,\theta,t)$ at four evolution times for an initially hollow plasma with an $l = 2$ seed. An $l = 2$ perturbation grows exponentially with an e-folding time of 17 μsec, and is clearly visible by $t = 50\ \mu$sec. At $t = 120\ \mu$sec, the mode is fully saturated, and would best be described as two isolated vortex structures with density plateaus about 50% above the density minima. The two vortices rotate around their own centers and around each other with both periods $\sim 10\ \mu$sec.

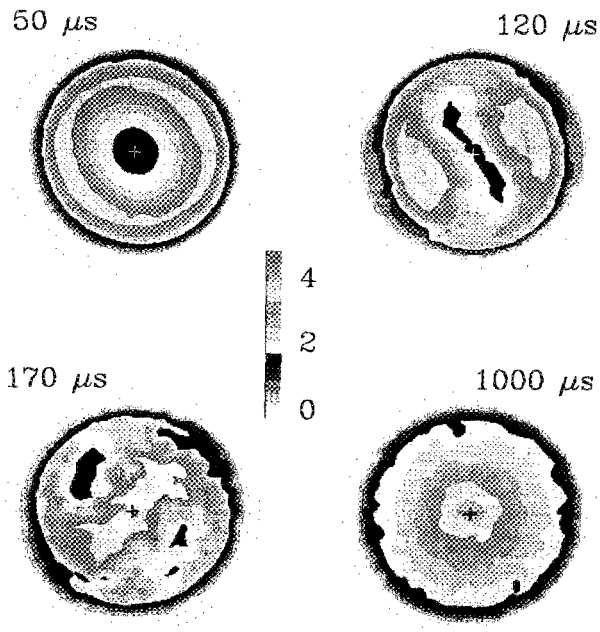

FIG. 10. Measured density $n(r,\theta)$ at four times in the evolution of a hollow column which had a small $l = 2$ perturbation at $t = 0$. Density units are 10^6 cm^{-3}.

The two vortices persist for many rotations, then begin to merge toward the center at $t = 170\,\mu$sec. Presumably, the two-vortex state is unstable, and the merger is the result of a vortex pairing instability.[18–20] There may be extended filamentary structures arising during the vortex formation and disintegration, as suggested, giving rise to density fluctuations on smaller spatial scales. Finally, by 1000 μsec the density is monotonically decreasing and therefore stable, and only small fluctuations are observed.

Mode eigenfunctions and amplitudes for the stable and unstable $l = 2$ modes can be obtained[9] by the process described above. We find that the stable mode has eigenfunction $\delta n_{2s} \approx r\,\partial n_0/\partial r$, and that the unstable mode eigenfunction δn_{2u} appears qualitatively similar to the eigenfunction δn_{1u}. Again, the two $l = 2$ mode frequencies differ widely. The amplitude of the stable $l = 2$ mode varies little during the linear phase of evolution, whereas the unstable mode e-folds every four wave periods until saturation.

These mode frequencies and growth rates are not well predicted by eigenvalue analysis with the step profile approximations of Fig. 3. Of course, instability is predicted only for hollow profiles, in agreement with observations. However, the completely hollow profile of Fig. 3(b) gives two complex conjugate modes, whereas two distinct mode frequencies are observed. Adding an internal step as in Fig. 3(c) does not change the prediction of conjugate modes, and small internal densities of $n_i \gtrsim 0.2$ can lead to a prediction of stability, whereas instability is observed even for barely hollow continuous profiles. The instability seems to be sensitive to $\partial n/\partial r$ at the resonant radii, which is not included in the step profile approximation. Approximating a continuous profile by a large number of steps brings in more modes, which are not observed experimentally.

Numerical solution of the eigenvalue equation for realistic smooth profiles has given fair agreement with unstable $l = 2$ growth rates in preliminary experiments. Computationally, the unstable mode is distinct from the continuum of eigenvalues which are the extension of the step profile to an infinite number of steps.

We note that the linear diocotron instabilities do not result in radial transport, but merely in rearrangement in θ. The instability saturates with the formation of two nonlinear vortices, and it is the dynamics of these secondary vortices that gives radial transport to a stable profile.

VII. TWO-VORTEX INTERACTION

The two-vortex merger process can be studied as an isolated process, independent of any diocotron instability process. Straightforward manipulation techniques allow us to form an initial condition consisting of two electron columns of chosen profile and placement. Here, we consider the particular case of two equal columns that are placed symmetrically on either side of the cylindrical axis, separated by a distance $2D$. Each vortex has a half-density radius of $R_p \approx 0.6$ cm.

We observe that the behavior of the two vortices depends dramatically on their separation to diameter ratio, i.e., $2D/2R_p$.[25] If the vortices are separated by more than 2.0 diameters, we observe that they orbit around each other rela-

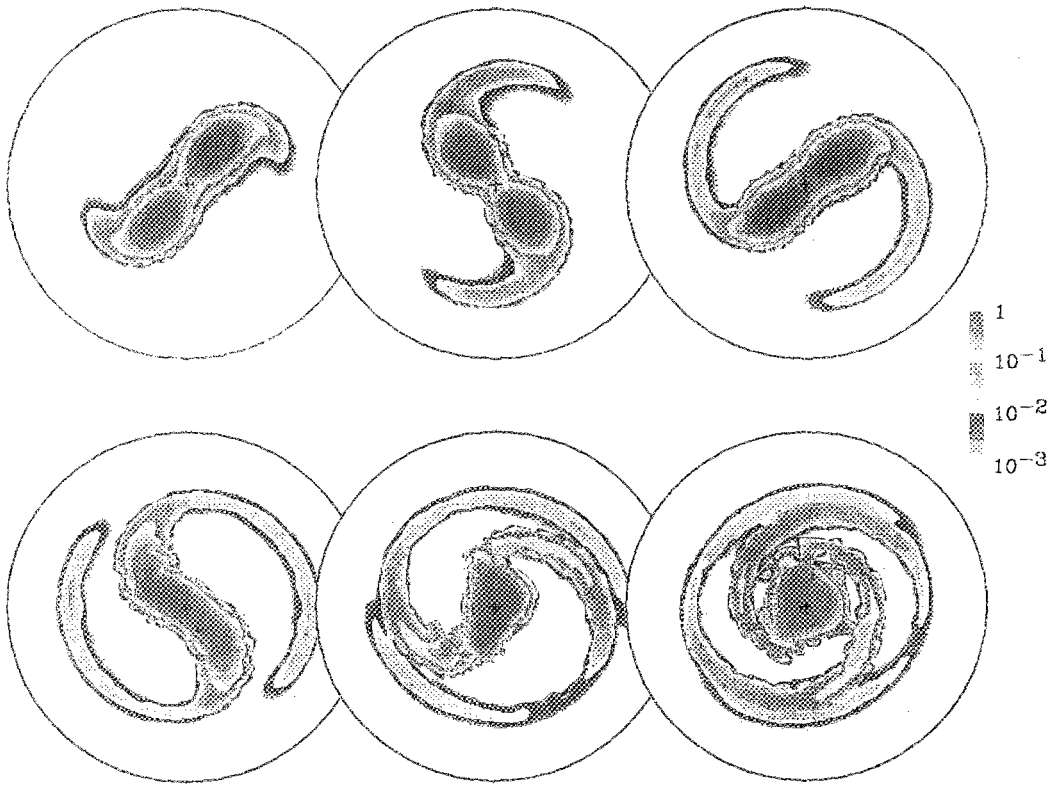

FIG. 11. Measured density $n(r,\theta)$ at six times during the merger of two vortices initially separated by 1.8 vortex diameters. Time intervals are 10 μsec.

tively unperturbed for up to 10^4 orbits. If the vortices are initially separated by 1.9 diameters, their mutual interaction quickly results in filamentary tail formation, but the vortices still orbit around each other for about 100 orbits before merging at the center.

Figure 11 shows an evolution where the vortices are separated by 1.8 diameters. Here, we observe merger at the center in less than one orbit period. The time to merge abruptly increases from 10 μsec to about 1 sec as the separation varies from 1.8 to 2.0 diameters. Of course, these last two numbers would vary somewhat with a different definition of R_p, since the vortex "edge" is a significant fraction of the radius. This may represent the cleanest experimental measurement to date of this fundamental vortex interaction process, due to the low inherent viscosity of the plasma, and due to the total absence of boundary layers at the wall. These preliminary results[25] are in fair agreement with theory and computational results,[26-28] and with an experiment in a water tank.[19]

The orbit frequency and vortex shape distortion can also be measured as a function of separation of the two vortices. We find that the orbit frequency is well modeled by the interaction of two "point" vortices of appropriate total circulation (i.e., total charge per unit length axially), but the wall interaction must be included for large separations. We also find that the interacting vortices elongate toward each other even in the absence of merger. The elongation appears roughly consistent with various "moment models" and numerical calculations,[26-28] but the experimental data have not yet been analyzed in detail.

Of course, two vortices may merge even if they are not symmetric in size or placement. Experimentally, the asymmetry is easily controlled. Also, it is easy to take three vortices as the initial condition. Here, the parameter space is substantially larger, and chaotic behavior is often observed.

ACKNOWLEDGMENTS

The authors gratefully acknowledge the contributions of John Malmberg, Tim Mitchell, and X.-P. Huang to the experiments, and theory discussions by R. A. Smith, M. N. Rosenbluth, and R. W. Gould.

This research was supported by the Office of Naval Research, Contract No. N00014-82-K-0621, the National Science Foundation, Contract No. PHY87-06358, and the U.S. Department of Energy, Contract No. DE-FG03-85ER53199.

[1] R. H. Levy, Phys. Fluids **8**, 1288 (1965); **11**, 920 (1968).
[2] R. J. Briggs, J. D. Daugherty, and R. H. Levy, Phys. Fluids **13**, 421 (1970).
[3] R. C. Davidson, *Theory of Nonneutral Plasmas* (Benjamin, Reading, MA, 1974), Sec. 2.10.
[4] J. H. Malmberg, C. F. Driscoll, B. Beck, D. L. Eggleston, J. Fajans, K. S. Fine, X.-P. Huang, and A. W. Hyatt (and other papers), in *Non-neutral Plasma Physics*, edited by C. W. Roberson and C. F. Driscoll (American Institute of Physics, New York, 1988), pp. 28–71.
[5] J. S. deGrassie and J. H. Malmberg, Phys. Fluids **23**, 421 (1980).
[6] W. D. White, J. H. Malmberg, and C. F. Driscoll, Phys. Rev. Lett. **49**, 1822 (1982).
[7] S. A. Prasad and T. M. O'Neil, Phys. Fluids **26**, 665 (1983); **27**, 206 (1984).
[8] G. Rosenthal, G. Dimonte, and A. Y. Wong, Phys. Fluids **30**, 3257 (1987).
[9] C. F. Driscoll, J. H. Malmberg, K. S. Fine, R. A. Smith, X.-P. Huang, and R. W. Gould, in *Plasma Physics and Controlled Nuclear Fusion Research 1988* (IAEA, Vienna, 1989), Vol. 3, pp. 507–514.
[10] K. S. Fine, C. F. Driscoll, and J. H. Malmberg, Phys. Rev. Lett. **63**, 2232 (1989).
[11] C. F. Driscoll, Phys. Rev. Lett. **64**, 645 (1990).
[12] W. Kelvin, Philos. Mag. (5), x. 155 (1880) [Papers, iv. 152].
[13] H. Aref, Annu. Rev. Fluid Mech. **15**, 345 (1983).
[14] J. W. S. Rayleigh, Proc. London Math. Soc. **11**, 57 (1880).
[15] R. L. Panton, *Incompressible Flow* (Wiley–Interscience, New York, 1984), Chap. 22.
[16] H. F. Webster, J. Appl. Phys. **26**, 1386 (1955).
[17] R. A. Smith and M. N. Rosenbluth, Phys. Rev. Lett. **64**, 649 (1990).
[18] J. C. McWilliams, J. Fluid Mech. **146**, 21 (1984).
[19] R. W. Griffiths and E. J. Hopfinger, J. Fluid Mech. **178**, 73 (1987).
[20] M. V. Melander, N. J. Zabusky, and J. C. McWilliams, J. Fluid Mech. **195**, 303 (1988).
[21] C. F. Driscoll, J. H. Malmberg, and K. S. Fine, Phys. Rev. Lett. **60**, 1290 (1988).
[22] W. Kelvin, Nature **23**, 45 (1880).
[23] R. T. Pierrehumbert, J. Fluid Mech. **99**, 129 (1980).
[24] H. Lamb, *Hydrodynamics* (Dover, New York, 1932), 6th ed., p. 232.
[25] K. S. Fine, C. F. Driscoll, T. B. Mitchell, and J. H. Malmberg, Bull. Am. Phys. Soc. **34**, 1932 (1989).
[26] K. V. Roberts and J. P. Christiansen, Comput. Phys. Commun. **3**, 14 (1972).
[27] P. G. Saffman and R. Szeto, Phys. Fluids **23**, 2339 (1980).
[28] M. V. Melander, N. J. Zabusky, and A. S. Styczek, J. Fluid Mech. **167**, 95 (1986).

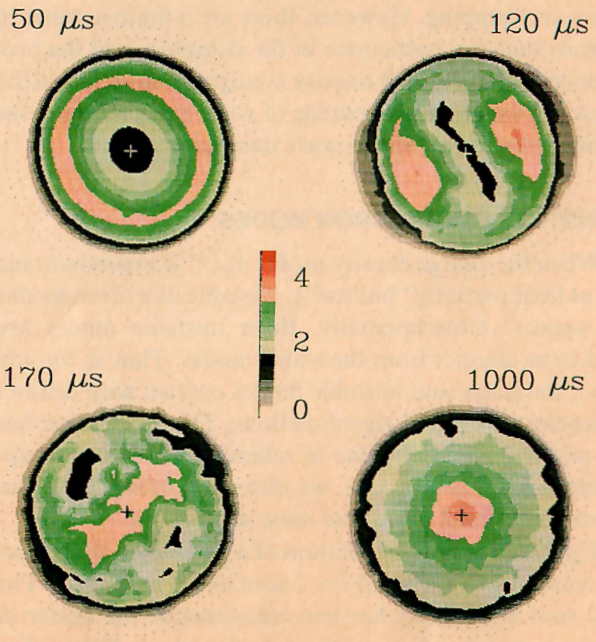

FIG. 10. Measured density $n(r,\theta)$ at four times in the evolution of a hollow column which had a small $l = 2$ perturbation at $t = 0$. Density units are 10^6 cm^{-3}.

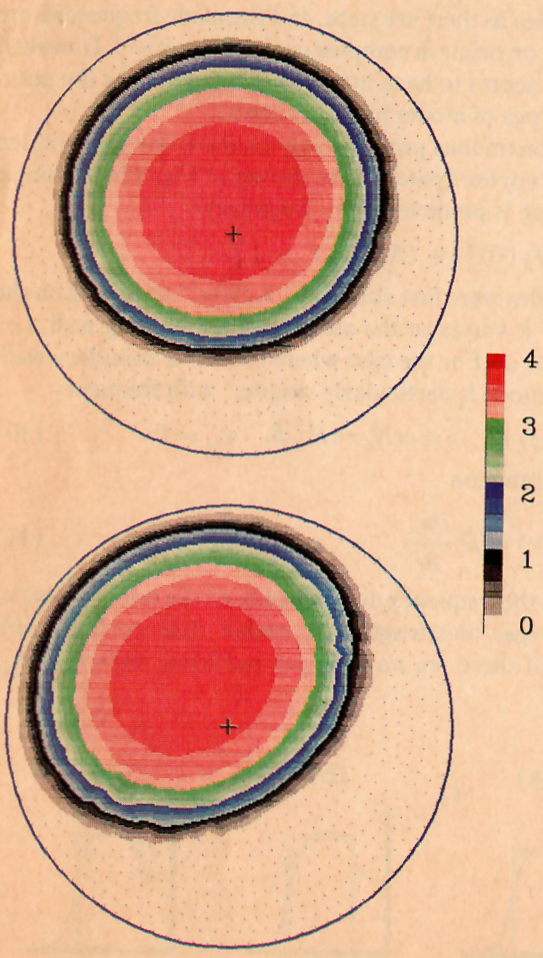

FIG. 4. Measured density $n(r,\theta)$ phase coherent with a stable $l = 1$ diocotron mode of two different amplitudes. Colors represent density on a linear scale of 10^6 cm^{-3}.

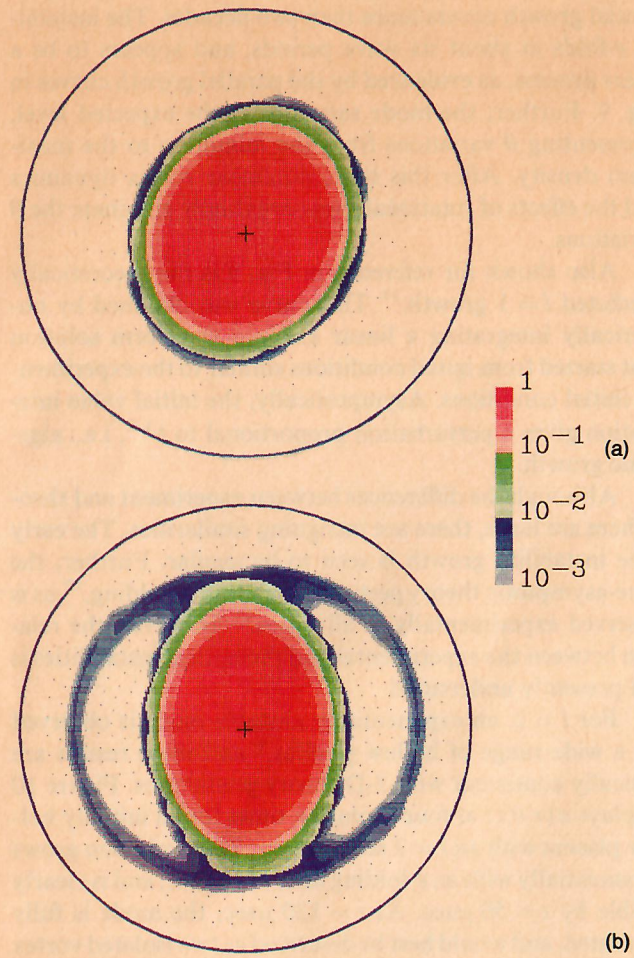

FIG. 6. Measured density $n(r,\theta)$ phase coherent with a stable $l=2$ diocotron mode of two different amplitudes. Colors represent density on a logarithmic scale.

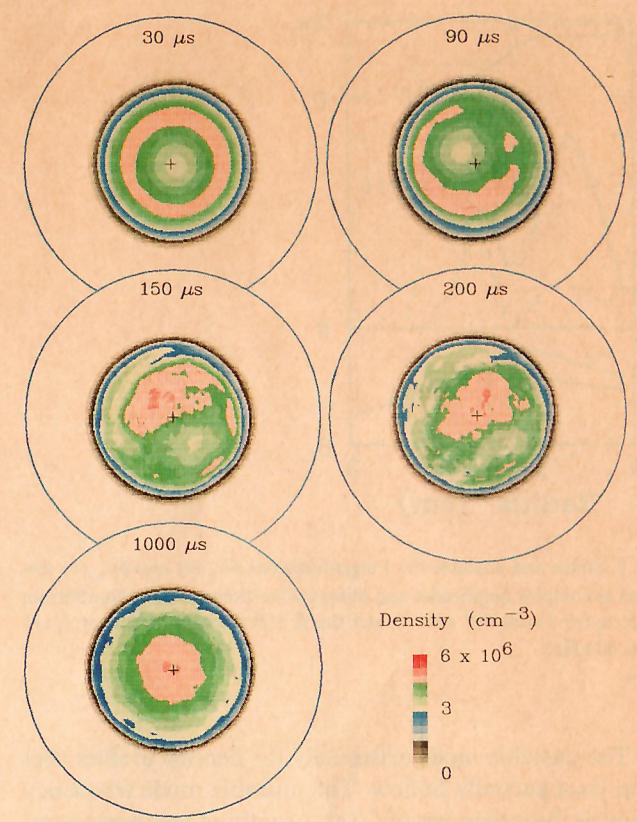

FIG. 7. Measured density $n(r,\theta)$ at five times in the evolution of a hollow column that had a small $l=1$ perturbation at $t=0$.

the low-density region orbits about the c.m. but it is spiraling outward with time (this is the unstable mode). The unstable mode also causes the high-density ring to collapse in θ into a

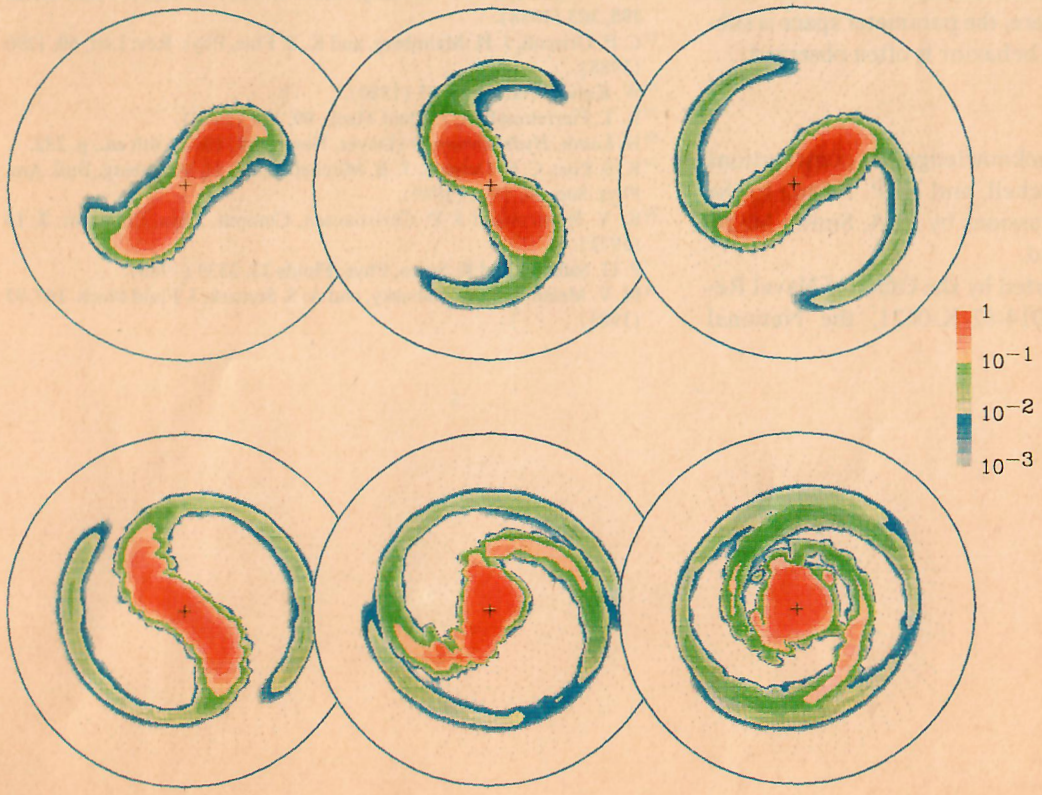

FIG. 11. Measured density $n(r,\theta)$ at six times during the merger of two vortices initially separated by 1.8 vortex diameters. Time intervals are 10 μsec.